catalysts

MDPI

Article

Role of Vanadium in Thermal and Hydrothermal Aging of a Commercial V_2O_5-WO_3/TiO_2 Monolith for Selective Catalytic Reduction of NOx: A Case Study

Luca Consentino [1], Giuseppe Pantaleo [1,*], Valeria La Parola [1], Eleonora La Greca [1,2], Nunzio Gallì [1], Giuseppe Marcì [3], Roberto Fiorenza [2,4], Salvatore Scirè [2,4] and Leonarda Francesca Liotta [1,*]

1 Institute for the Study of Nanostructured Materials (ISMN), National Research Council (CNR), Via Ugo La Malfa 153, 90146 Palermo, Italy; luca.consentino@ismn.cnr.it (L.C.); valeria.laparola@cnr.it (V.L.P.); eleonora.lagreca@ismn.cnr.it (E.L.G.); nunzio.galli@cnr.it (N.G.)
2 Department of Chemistry, University of Catania, Viale A. Doria 6, 95125 Catania, Italy; roberto.fiorenza@unict.it (R.F.); sscire@unict.it (S.S.)
3 "Schiavello-Grillone" Photocatalysis Group, Department of Engineering, University of Palermo, Viale delle Scienze, 90128 Palermo, Italy; giuseppe.marci@unipa.it
4 Interuniversity Consortium in Chemical Reactivity and Catalysis (C.I.R.C.C.), University of Catania Research Unit (UdR of Catania), Viale A. Doria 6, 95125 Catania, Italy
* Correspondence: giuseppe-pantaleo@cnr.it (G.P.); leonardafrancesca.liotta@cnr.it (L.F.L.)

Abstract: In recent years, increased attention to air pollutants such as NO_x has led the scientific community to focus meaningfully on developing strategies for NO_x reduction. Selective catalytic reduction of NO_x by ammonia (NO SCR by NH_3) is currently the main method to remove NO_x from diesel engine exhaust emissions. The catalysts with typical V_2O_5-WO_3/TiO_2 (VWTi) composition are widely used in NH_3-SCR for their high NO_x conversion activity, low cost, and robustness, especially concerning sulfur poisoning. However, in real diesel engine working conditions, the thermal and hydrothermal aging of catalysts can occur after several hours of operation at high temperature, affecting the catalytic performance. In this study, the stability of a commercial VWTi monolith, self-supported and containing glass fibers and bentonite in its matrix, was investigated as a case study. In laboratory conditions, NO SCR tests were performed for 50 h in the range of 150 to 350 °C. Subsequently, the VWTi monolith was thermally and hydrothermally aged at 600 °C for 6 h. The thermal aging increased the NO_x conversion, especially at low temperature (<250 °C), while the hydrothermal aging did not affect the SCR. The differences in NO_x conversion before and after aging were associated with the change in vanadium and tungsten oxide surface coverage and with the reduction in the surface area of catalysts. In order to correlate the change in SCR activity with the modifications occurring after aging processes, the monolithic samples were characterized by several techniques, namely XRD, SSA and pore analysis, TPR, XPS, Raman, TGA and SEM/EDX.

Keywords: V_2O_5-WO_3-TiO_2 monolith; hydrothermal aging; NO SCR; ammonia

Citation: Consentino, L.; Pantaleo, G.; La Parola, V.; La Greca, E.; Gallì, N.; Marcì, G.; Fiorenza, R.; Scirè, S.; Liotta, L.F. Role of Vanadium in Thermal and Hydrothermal Aging of a Commercial V_2O_5-WO_3/TiO_2 Monolith for Selective Catalytic Reduction of NOx: A Case Study. *Catalysts* **2024**, *14*, 241. https://doi.org/10.3390/catal14040241

Academic Editors: Ioannis V. Yentekakis and Keith Hohn

Received: 9 February 2024
Revised: 25 March 2024
Accepted: 3 April 2024
Published: 5 April 2024

1. Introduction

The nitrogen oxides (NO_x) from exhaust emissions of engines are well-known to be harmful to human health and the environment [1]. For this reason, several stringent regulations and laws have been issued in many parts of the world to limit the pollutant emissions produced by diesel engines. Exhaust gas aftertreatment systems effectively eliminate pollutants from internal combustion engines' exhausts without compromising engine power or fuel efficiency. Among these systems, selective catalytic reduction (SCR) systems are utilized in both road and marine applications to significantly reduce NO_x emissions [2]. SCR systems can operate independently and exhibit high reliability and durability without requiring significant engine alterations. In the standard SCR reaction,

the ammonia reduces nitrogen oxides (e.g., NO) to nitrogen over a solid catalyst according to Equation (1) [3]:

$$4NO + 4NH_3 + O_2 \rightarrow 4N_2 + 6H_2O \quad (1)$$

A variety of SCR catalytic systems have been investigated, including zeolites (such as Fe-ZSM-5 and Cu-CHA zeolite) [4,5], noble metals (such as Ag, Pd, and Pt) [6,7], and metal oxides (such as V-Mo/TiO_2, V-Nb/TiO_2, and V-W/TiO_2) [8–10]. Among these categories, metal-oxide-based catalysts are the most commonly utilized, with vanadia-tungsten supported titania catalysts being particularly prominent because of their elevated conversion efficiencies in the medium-high temperature range (250–400 °C), strong sulfur resistance and low costs [11]. In this type of catalyst, TiO_2 is commonly present as anatase and acts as support material, and around 10 wt% WO_3 is introduced as a promoter of catalyst stability and surface acidity [12–15]. Vanadium oxide species, reported as V_2O_5 ca. 1–3 wt% [3], represent a redox-active component [13,16,17] and are responsible for the SCR activity [18].

Excellent results have been reported by Napolitano et al. [2] using VWTi catalysts for NO_x conversions in maritime applications within a fixed temperature range. However, the land-based diesel vehicle engines do not operate under established working conditions and hence can be subjected to unexpected temperature fluctuations. In this case, the evaluation of thermal stability for SCR catalysts is crucial to endure harsh conditions. The temperatures of the diesel exhaust are often higher than 650 °C due to the periodic regeneration diesel particulate filter (DPF) necessary to eliminate particulate matter (PM) [19]. The NH_3-SCR reactor is usually located downstream of the DPF to meet the current strict emission standards [20,21], causing the exposure of SCR catalyst to high temperatures and humidity [22,23]. In these conditions, VWTi catalysts can undergo a loss in activity due to the phase change of TiO_2 from anatase to rutile above 550 °C [24]. Moreover, there is concern that vanadium species could be released at those temperatures as a result of washcoat delamination [25] or volatilization [20,26,27], posing potential risks to human health and the environment [28,29]. For all of these reasons, it is crucial to understand the thermal and hydrothermal stability of vanadia-based catalysts in detail.

The influence of time and temperature on catalyst morphology and activity during thermal aging was examined by Kompio et al. [14]. They reported that in the aging temperature range between 600 and 750 °C, a VWTi catalyst with low V_2O_5 loading (0.5–1.5 wt%) can be thermally activated or deactivated depending on the aging time. It was found, for instance, that VWTi catalysts aged at 600 °C showed higher performance than in the fresh state. However, increasing the aging temperature, the same catalysts underwent a heavy deactivation after 1000 min. The same increased SCR activity for low V-loaded VWTi has been reported by other researchers in recent years [30–32]. The structural change, the formation of bulk WO_3 and polymeric VO_x species, seems to play a key role in increasing the activity upon aging of the catalysts [13,33,34]. However, high V-loaded (3 wt%) VWTi showed decreased SCR activity owing to a significant diminution of surface area after aging [30].

Regarding hydrothermal aging, there are many studies focusing on the vanadia SCR-catalyst [31,32,35]. Asako et al. [36] aged vanadia catalyst for 100 h at 550 °C and found that it lost 40−60% of its activity. Madia et al. [30] performed progressive aging experiments for 100 h at 550 °C and 30 h at 600 °C and found that 2 wt% V_2O_5 had the best hydrothermal stability. Rasmussen and Abrams [37] demonstrated that vanadium tungsten catalyst was stable under hydrothermal conditions at 550 °C (110 h). Maunula et al. [38] found good durability without deactivation using 10% H_2O up to 750 °C for 20 h.

Although a significant amount of research has been conducted on hydrothermal aging of vanadium-based catalysts, certain areas remain controversial. Only a few studies have specifically examined changes to the active sites during hydrothermal aging. Works in the literature proposed that the presence of water can result in a decrease in activity due to competition with ammonia for adsorption [39–41].

This study aimed to understand the effect of realistic, brief thermal-hydrothermal aging on state-of-the-art V-SCR catalysts. Even though it is widely known that V-SCR catalysts should not be exposed to exhaust temperatures above 550 °C, there is a possibility that brief high-temperature events caused by engine malfunctions or rapid hydrocarbon decomposition may exceed this limit. By investigating the impact of short-term hydrothermal aging on the morphology, chemical composition, and catalytic performance of a state-of-the-art V-SCR catalyst, this study can provide valuable information on the real-world impact of brief high-temperature events. In this work, the stability of a commercial VWTi monolith, cordierite-free, but containing glass fibers and bentonite in the matrix in order to ensure its honeycomb structure, was investigated in laboratory conditions as a case study. NO SCR tests were carried out between 150 and 350 °C for 50 h. Subsequently, the catalytic performances of the monolith were studied after thermal and hydrothermal aging at 600 °C for 6 h in dry and wet conditions. Several characterization techniques (XRD, SSA and pores analysis, TPR, XPS, Raman, TGA and SEM/EDX) were used to correlate the change in SCR activity with the modifications occurring after aging processes.

2. Results and Discussion

2.1. Catalytic Activity

VWTi monolith was tested as received to evaluate its NO conversion and N_2 selectivity (see black curve in Figures 1 and 2) in a standard NO-SCR test in which the data points were collected after waiting 40 min at each temperature. Temperatures above 400 °C were not investigated because NH_3 oxidation occurs, influencing the real conversion and selectivity evaluation. [14,31]. NO conversion increased between 125 and 200 °C, and a conversion of over 90% was reached between 220 and 400 °C (Figure 2). Similarly, nitrogen selectivity remained consistently high between 100 °C and 350 °C, marginally decreasing to 95% at 400 °C (Figure 2). The catalytic behavior exhibited by the VWTi monolith was in accordance with what has been reported in the literature [2,18]. Accurately defining its performance was crucial for subsequent stability and aging studies.

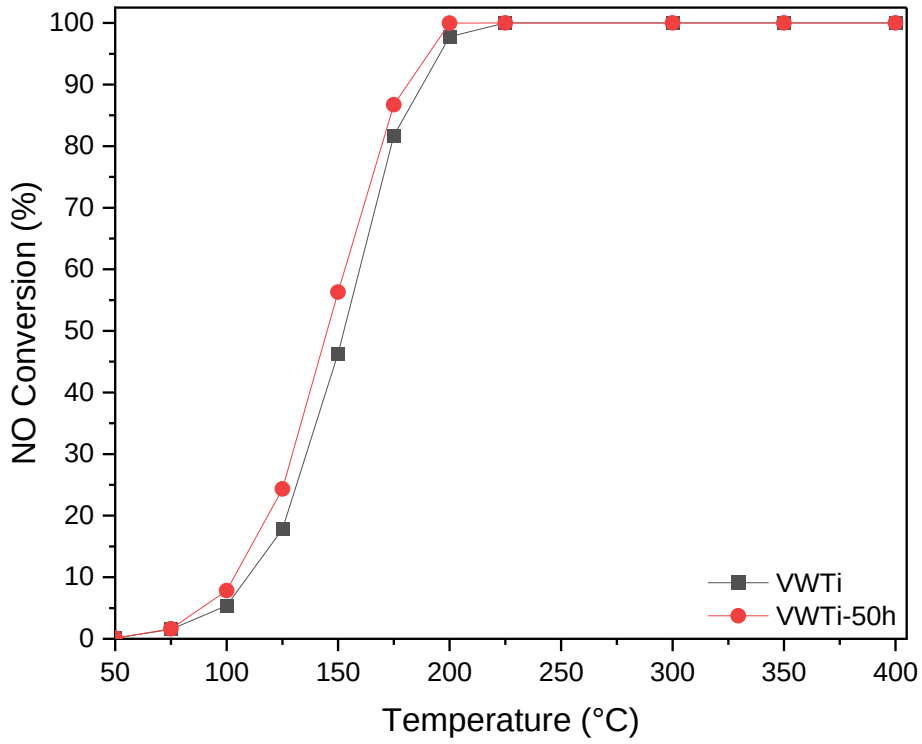

Figure 1. NO conversion over VWTi and VWTi-50 h monolithic catalysts.

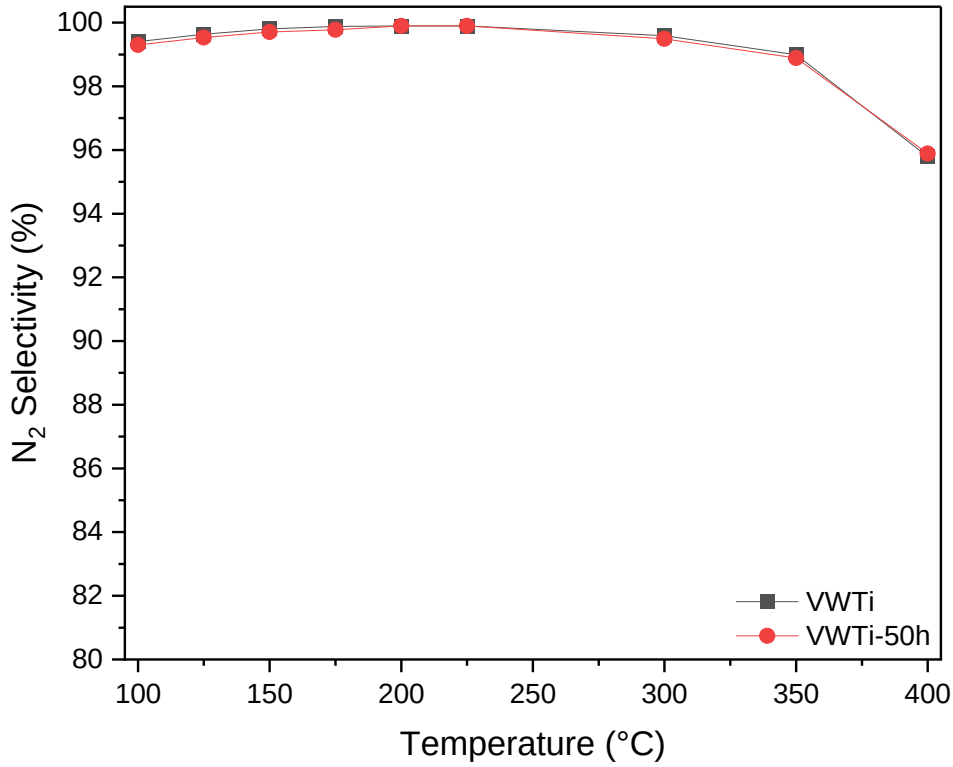

Figure 2. N_2 selectivity over VWTi and VWTi-50 h monolithic catalysts.

The long run test was performed over a total of 50 h, in which each temperature was maintained for 5 h, except for the critical temperatures of 350 and 200 °C, which were maintained for 12 h. These two temperatures, indeed, represent the extremes that define the maximum conversion and selectivity range (as showed in Figures 1 and 2). For that reason, a longer observation time was chosen. Figure 3 displays the profile of NO concentration in parts per million (ppm) as a function of time, at different reaction temperatures. At the end of the NO-SCR test, the temperature of VWTi monolith was lowered to 350 °C and maintained for 12 h, resulting in a NO concentration of zero ppm. The same trend was observed by decreasing the reaction temperature by steps of 25 °C until reaching 200 °C, as expected from the conversion graph in Figure 1. At 175 °C and 150 °C, a noticeable increase in NO concentration (approximately 25 and 250 ppm, respectively) was observed, in accordance with the diminished catalyst activity at lower temperatures, as shown in Figure 1. Furthermore, to validate that the VWTi retained its performance after 50 h of continuous reaction, a standard SCR test was conducted after the long run (refer to red curve in Figures 1 and 2). The selectivity for nitrogen remained identical to those obtained before the 50 h long run test, while the conversion exhibited a slight increase between 150 and 200 °C. This behavior could be attributed to aging-induced activation over the 50 h period, a phenomenon that will be further explored in this section.

The stability test over 50 h of the VWTi monolith revealed crucial insights into its long-term performance. Evaluating how the catalyst maintains its efficiency and selectivity over an extended period is vital for understanding its practical applicability and durability in real-world applications. This analysis helps determine whether the catalyst can sustain its effectiveness without significant degradation or loss of catalytic activity, ensuring its reliability and functionality over time.

However, envisaging practical applications, it is not only important to assess the stability of the catalyst over time, but also its robustness concerning aging phenomena that may occur due to temperature spikes or the presence of water. For this reason, the impact of thermal and hydrothermal aging at 600 °C for 6 h on the catalytic activity of VWTi was

investigated, and NO-SCR tests were carried out over the aged monoliths (Figures 4 and 5). The temperature of 600 °C was chosen to guarantee deactivation [30].

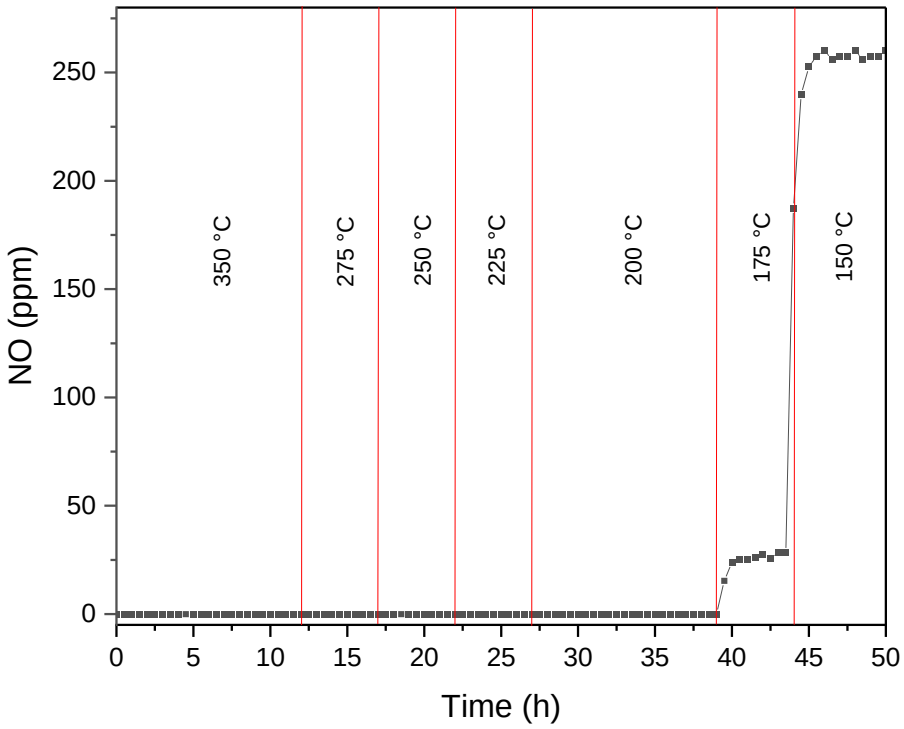

Figure 3. NO concentration (ppm) profile as a function of time (h) at various temperatures over VWTi during a long run of 50 h.

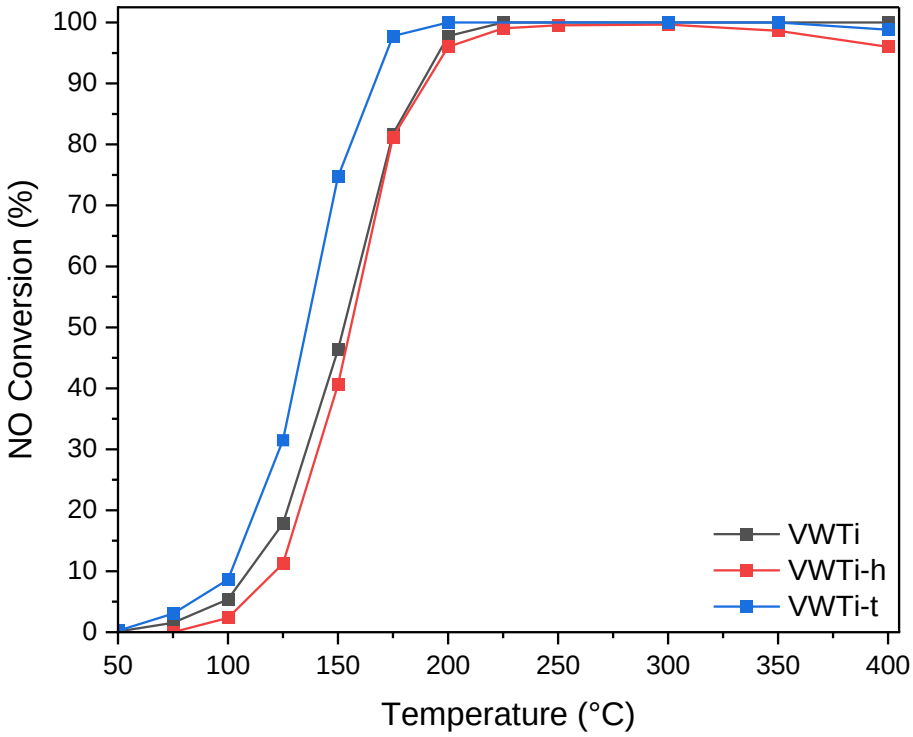

Figure 4. NO conversion over VWTi, VWTi-h and VWTi-t monolithic catalysts.

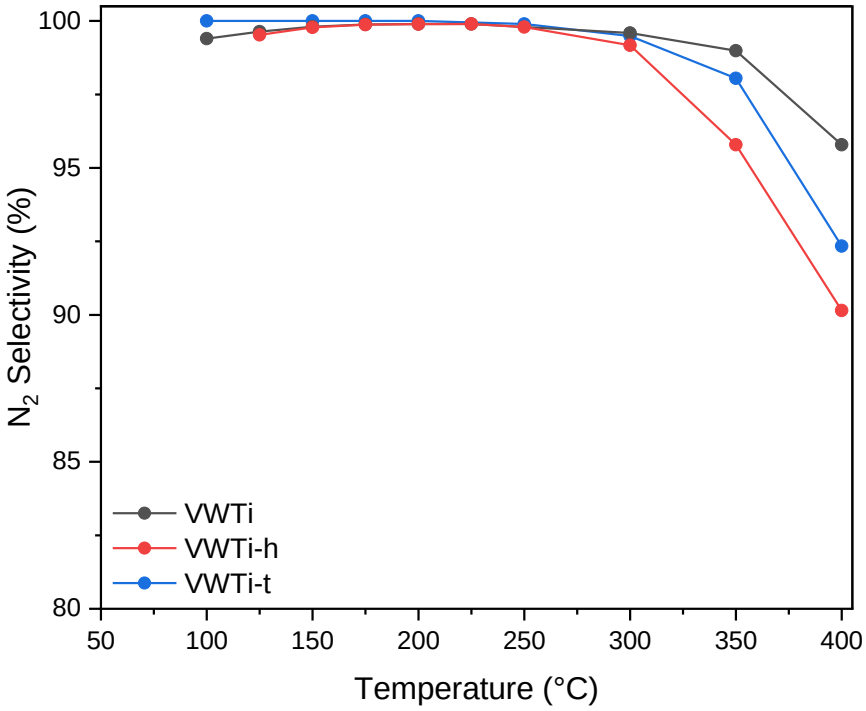

Figure 5. N_2 selectivity over VWTi, VWTi-h and VWTi-t monolithic catalysts.

After hydrothermal aging, the monolithic sample, labelled as VWTi-h, showed in a subsequent standard NO-SCR test only a slight decrease in NO conversion between 75–150 °C, leaving activity at high temperature almost unchanged, except at higher temperature (350–400 °C), while a pronounced decay in the selectivity for N_2 was registered above 300 °C. Conversely, the thermally aged catalyst, VWTi-t, showed improved NO conversion at low temperature (75–200 °C) compared to hydrothermally aged and fresh samples, while at 350–400 °C, the N_2 selectivity decreased, but to a lesser extent than for the hydrothermally treated catalyst. Similar effects in the NO SCR performance of V-loaded VWTi catalysts have been already reported in the literature [30–32] and have been attributed to several factors, especially the formation of bulk WO_3 and polymeric VOx species that are favored by sintering of the TiO_2 support and seem to play a key role in increasing the activity upon aging of the catalysts [13,33,34].

In order to explain the so far discussed modifications in NO SCR and with the aim to detect structural, morphological, redox and electronic changes occurring during the aging process, detailed characterizations of the monoliths were carried out as reported below.

2.2. X-ray Diffraction

The phase composition and structural characteristics of the VWTi, VWTi-t and VWTi-h catalysts were investigated using X-ray diffraction (XRD), and their patterns are presented in Figure 6. The XRD patterns of all three samples indicated the presence of two crystalline phases of TiO_2, mainly anatase (ICSD file n. #9854) and rutile (ICSD file n. #9161), which were confirmed by comparison with the ICSD references. No evident sintering and transformation from anatase to the rutile phase occurs in the TiO_2 structure upon hydrothermal or thermal aging.

Interestingly, the studied catalysts showed no discernible peaks that could be attributed to the WO_3 and V_2O_5 phases, neither before nor after hydrothermal and thermal aging. This implies that these species may exist in catalysts as finely dispersed oxides or in an unordered state, consistent with previous research results [2].

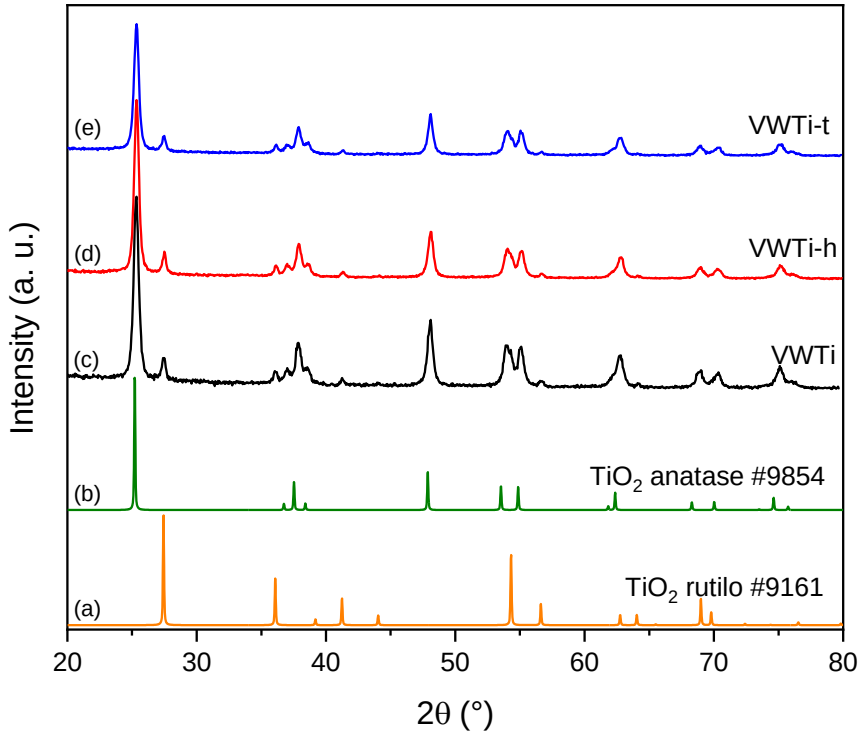

Figure 6. XRD patterns of (a) TiO_2 rutile (ICSD file n. #9161), (b) TiO_2 anatase (ICSD file n. #9854), (c) VWTi, (d) VWTi-h and (e) VWTi-t.

2.3. Specific Surface Area and Pores

The N_2 adsorption/desorption isotherms were registered over the samples in order to calculate the specific surface area (SSA), pore volume and mean pore size distribution. The values are listed in Table 1. Upon hydrothermal aging, a decrease in the surface area (from 53 to 37 $m^2\ g^{-1}$) and the formation of larger pores (24.9 vs. 15.8 nm) took place in comparison with the fresh sample, pointing to a sintering effect [31,42]. Conversely, thermal aging induced increased surface area (from 53 to 60 $m^2\ g^{-1}$) that was accompanied by higher pore volume, from 0.26 to 0.34 $cm^3\ g^{-1}$, and larger pore size (20.6 vs. 15.8 nm) with respect to the as received catalyst, suggesting structural changes and redispersion of surface-active species that likely rearrange in a more porous network.

Table 1. Textural properties of the monolithic catalysts.

Samples	Surface Area ($m^2\ g^{-1}$)	Pore Volume ($cm^3\ g^{-1}$)	Mean Pore Size (nm)
VWTi	53.0	0.26	15.8
VWTi-h	60.0	0.34	20.6
VWTi-t	37.0	0.25	24.9

2.4. H_2-TPR

The redox properties of the monolithic catalysts (VWTi, VWTi-t and VWTi-h) were investigated by H_2-TPR measurements. As shown in Figure 7, the hydrogen consumption peaks can be divided into two main zones. Considering VWTi monolith, the first peak, between 450 and 550 °C, corresponded to the reduction of V^{5+} species to V^{3+} and was indicative of highly dispersed vanadium species [43], while the shoulder at 410 °C was associated with polymeric aggregates. The second main peak, between 750 and 900 °C, corresponded to the reduction of W^{6+} to W^{4+} species [7,38]. An intermediate reduction zone, centered at around 630 °C, was also detected, corresponding to the reduction of well-dispersed V-O-W species. Regarding the aged samples (VWTi-t and VWTi-h), they

both exhibited two main peaks of reduction in the same ranges of temperature along with a reduction feature near 630 °C. However, it should be noted that the first peak, observed at 470 °C in the fresh sample, was shifted at around 520 °C upon aging. Moreover, such peak had a very broad shape, suggesting the reduction of a different type of vanadium species with not well-defined chemical environment. On this basis, it can be concluded that the aging process modified the structure and dispersion of vanadium oxidized species, as well as their interaction with the TiO_2 support. In Table 2 are reported the hydrogen consumption values and the range of temperatures of the main peaks. As can be observed, the experimental consumption of V and W exceeded their respective theoretical consumption due to the simultaneous reduction of part of the surface (at around 300–500 °C) and bulk (at around 850–900 °C) TiO_2 [44]. Furthermore, there was a progressive lowering of the experimental hydrogen consumption in the sequence: 26.5–25.6–22.8 mL g^{-1} for VWTi, VWTi-h, and VWTi-t, respectively. This can be explained considering that due to the sintering of titania upon hydrothermal and thermal aging, the exposed reducible surface area of the support and its total reducibility decreased.

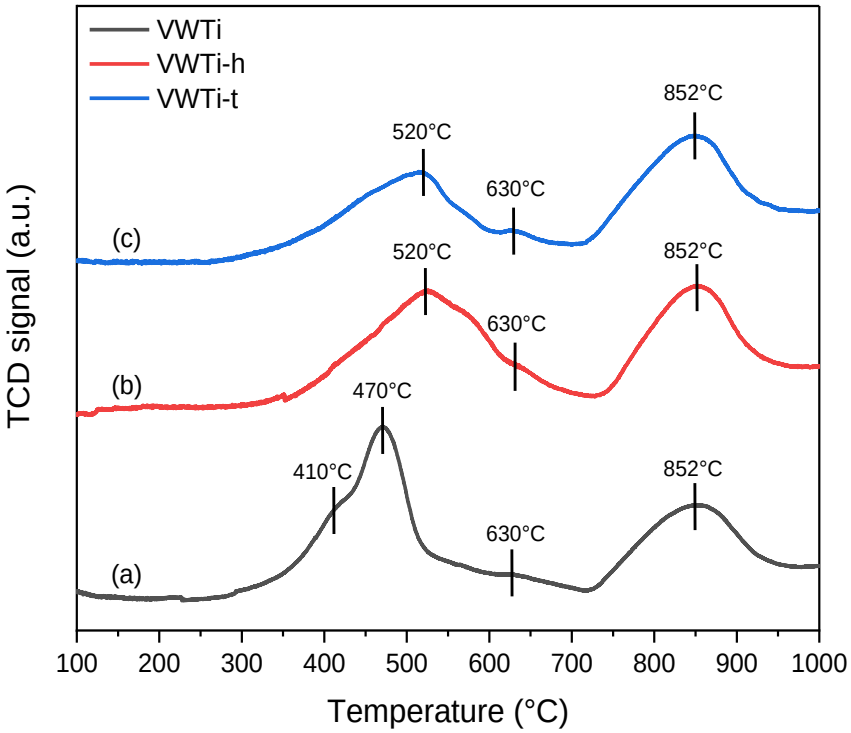

Figure 7. H_2-TPR profiles of (a) VWTi, (b) VWTi-h and (c) VWTi-t.

Table 2. Reduction temperatures and hydrogen consumption values of the monolithic catalysts.

Sample	Temperature Range (°C)	Experimental H_2 Consumption (mL g^{-1})	Theoretical H_2 Consumption (mL g^{-1})
VWTi	300–700	14.0	9.6 ($V_2O_5 \rightarrow V_2O_3$)
	700–1000	12.5	10.6 ($WO_3 \rightarrow WO_2$)
	Total	26.5	20.2
VWTi-h	400–700	10.9	9.6 ($V_2O_5 \rightarrow V_2O_3$)
	700–1000	14.7	10.6 ($WO_3 \rightarrow WO_2$)
	Total	25.6	20.2
VWTi-t	400–750	8.1	9.6 ($V_2O_5 \rightarrow V_2O_3$)
	700–1000	14.7	10.6 ($WO_3 \rightarrow WO_2$)
	Total	22.8	20.2

2.5. XPS

The XPS analysis was performed on the monolithic catalyst as slab in order to analyze the surface composition. Figure 8 shows the survey scan of the sample. The spectrum confirmed the presence of Ti, O, W, Si and Al, according with the chemical composition reported in the data sheet. The main peak relative to vanadium (V2p) overlapped with the more intense O1s satellites arising by the emission due to the Al Kα 3 component of the un-monochromatized radiation. This overlapping made its analysis subject to important errors (see blue inset in Figure 8).

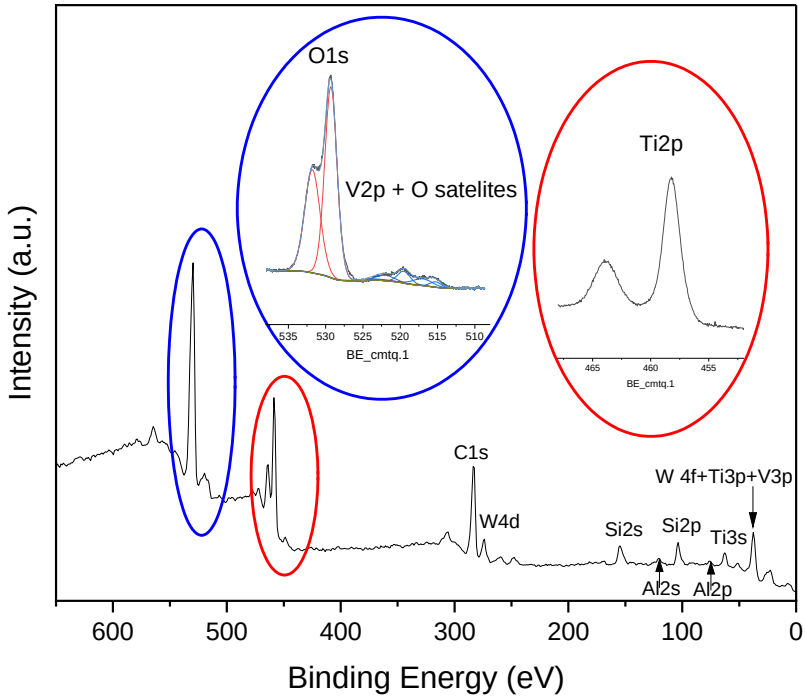

Figure 8. XPS survey spectrum of VWTi (as slab). In the blue inset, the O1s + V2p region; in the red inset, the Ti2p region.

On the contrary, the region between 30 and 50 eV contained clearly distinguishable peaks relative to W4f, Ti3p and V3p; for this reason, this region was used to analyze and quantify these elements. The results in terms of $W4f_{7/2}$, V3p, and O1s binding energies (eV) and surface W/Ti and V/Ti atomic ratios are listed in Table 3. Figure 9 shows the W4f, Ti3p and V3p regions of the monolith. The spectra show a complex peak that can be deconvoluted with two doublets, due to the spin orbit splitting of $W4f_{7/2}$ and $W4f_{5/2}$ (spin orbit separation = 2.1 eV), a peak attributed to Ti3p and a peak due to V3p. According to the literature, the position $W4f_{7/2}$ at 35.7eV is due to W(VI), while $W4f_{7/2}$ at 34.3 eV is due to W (V) [45–47]. By deconvolution of the region, it was found that tungsten was present as W(VI). The V3p position was in accord with the presence of V(V) [48–50]. Ti3p (37.2eV) was in accord with the presence of Ti (IV) [51,52]. This fact was confirmed by the analysis of the Ti2p region with the two typical peaks at 458.2 eV ($Ti2p_{3/2}$) and 463.9 eV ($Ti2p_{1/2}$) (see red inset in Figure 8) [53]. By looking at the atomic ratio of vanadium and tungsten with respect to titanium, an important surface enrichment was found. Upon treatments, no differences were found in the chemical state of the elements; nevertheless, a further surface enrichment of vanadium was found, especially for the VWTi-t sample. Oxygen showed the typical profile of TiO_2 material with a component at ca. 529.5 eV due to lattice and a component at 531.5 eV due to OH surface groups [53]. No trends were found in the relative changes of the two components after thermal or hydrothermal treatments (see Figure 10 and Table 3).

Table 3. XPS results in terms of W4f$_{7/2}$, V3p and O1s binding energies (eV) of the monolithic device and W/Ti and V/Ti atomic ratios. The relative intensities of the different components O1s are given in parentheses.

Sample	W 4f$_{7/2}$ (eV)	V3p (eV)	O1s	W/Ti (0.03) *	V/Ti (0.03) *
VWTi	35.8	41.0	529.3 (58%) 531.8 (42%)	0.23	0.13
VWTi-h	35.6	41.7	529.6 (64%) 531.6 (36%)	0.23	0.15
VWTi-t	36.0	41.4	529.4 (56%) 531.7 (44%)	0.17	0.22

* nominal ratio value.

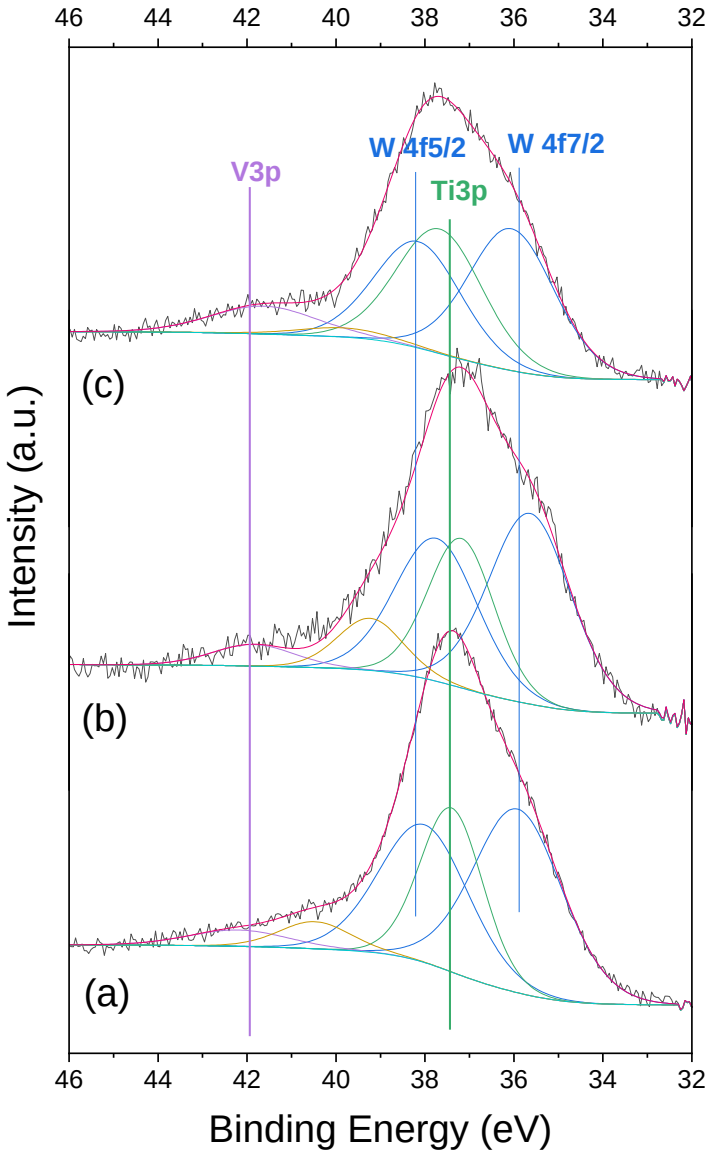

Figure 9. W4f, Ti3p and V3p region of VWTi (a), VWTi-h (b) and VWTi-t (c).

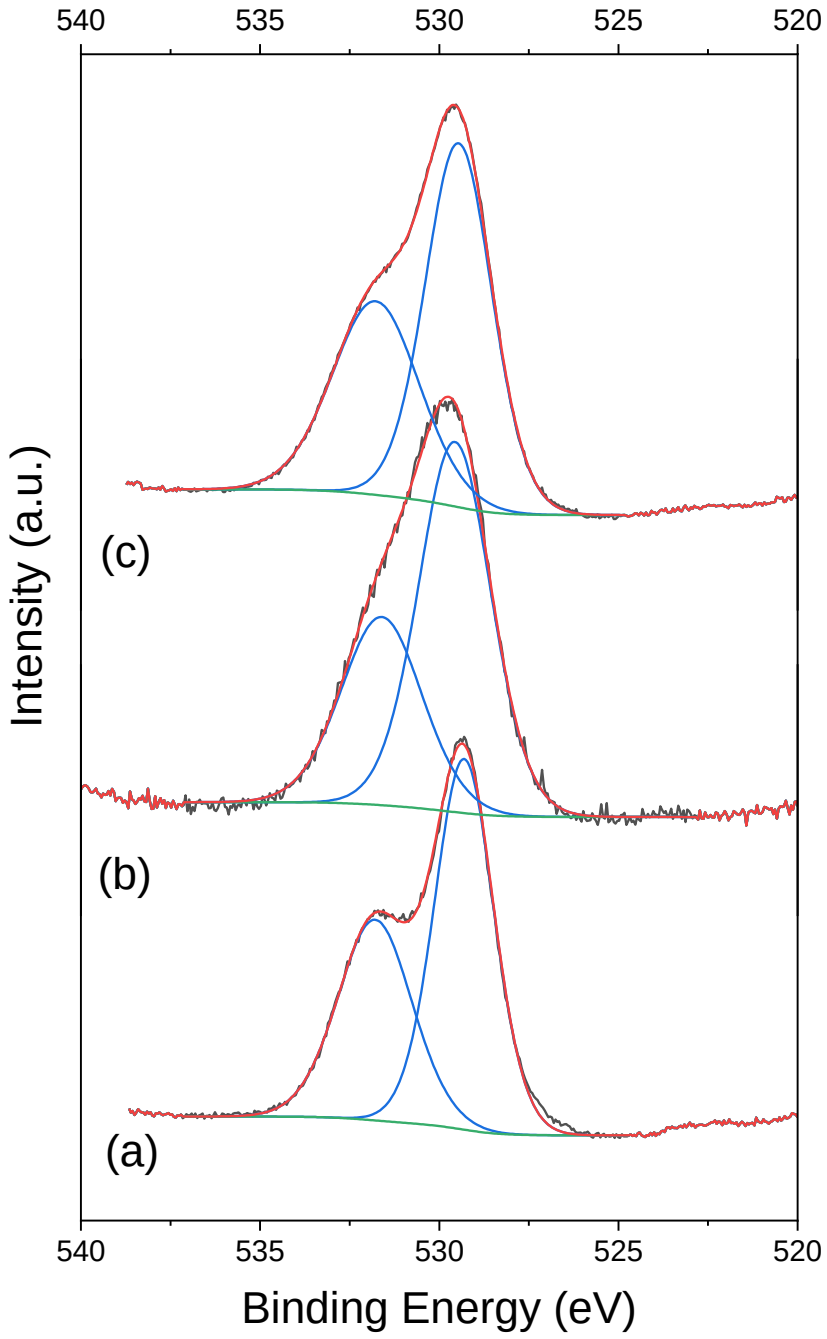

Figure 10. O1s region of VWTi (a), VWTi-h (b) and VWTi-t (c).

2.6. Raman Analysis

In order to gain more insight into the structure of VWTi catalysts and their modifications occurring upon aging, Raman analysis was also performed. The Raman spectra of the examined samples are reported in Figure 11A. All of the samples showed vibrational bands at around 149, 393, 514 and 636 cm^{-1}, typical of the TiO_2 in the anatase form [54]. Noteworthily, as reported for similar samples, the strong intensity of Raman bands related to anatase hindered the main bands associated with the vibrational modes of surface V_2O_5 and WO_3 species in the region below 800 cm^{-1} [54,55]. This can be related to the good dispersion of the vanadium and tungsten oxides and to their lower content compared to the TiO_2 (see Table 4), in accordance with the XRD measurements. Interestingly, the position of the main vibrational mode of anatase of the VWT-t sample (149 cm^{-1}, Figure 11B) showed a blue shift of 4 cm^{-1} compared to the VWT-h and VWT catalysts (145 cm^{-1}). This is

attributed to a lattice distortion of TiO_2 due to the introduction of defects as a consequence of the thermal treatment [56,57]. Furthermore, in the VWT-t sample, it was possible to note a broad signal in the 800–1000 cm^{-1} region. Considering the presence of a small band at 197 cm^{-1}, related to the bending vibrations of the O–V–O bond, the 800–1000 cm^{-1} signal can be assigned to the small contributions of the vanadium oxide surface species [57]. This pointed to the fact that the thermal treatment caused a surface segregation of the vanadium species in the VWT-t catalyst, as also confirmed by XPS. These structural modifications of the VWT-t sample could explain the higher activity of this catalyst in the NO conversion, especially at low temperatures, compared to the VWT and VWT-h samples.

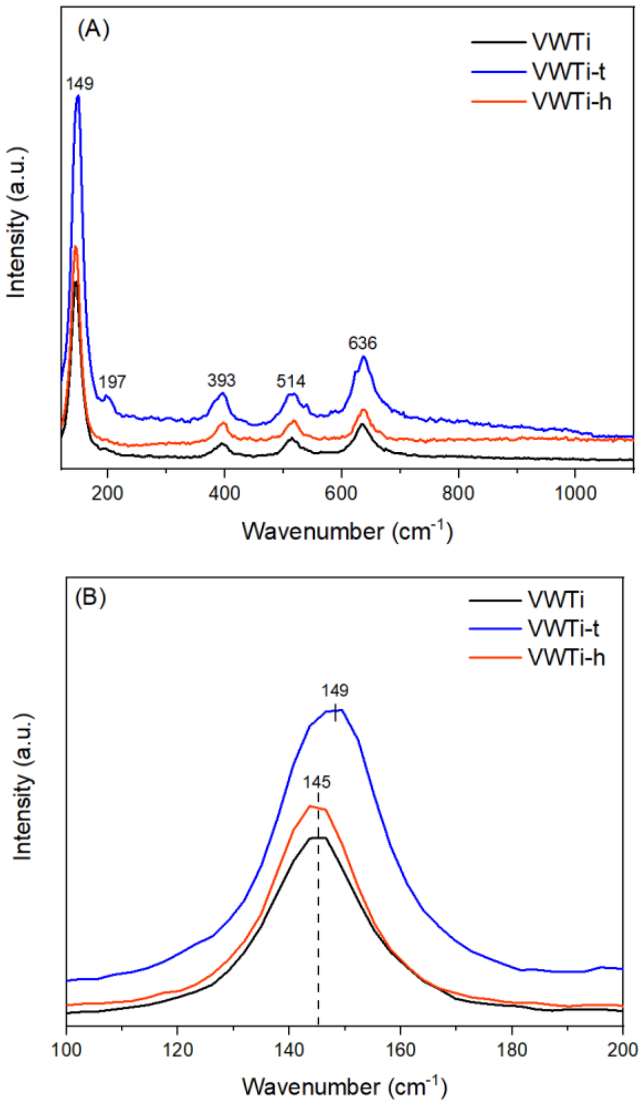

Figure 11. (**A**) Raman spectra of the examined samples. (**B**) Zoom of the 100−200 cm^{-1} region.

Table 4. Chemical composition of the commercial monolithic catalyst.

Phase	Wt%
TiO_2	75.0
WO_3	7.0
V_2O_5	3.0
bentonite	6.0
glass fiber	9.0

2.7. TGA Analysis

The TGA curves of fresh and aged catalysts are shown in Figure 12. In the temperature range of 25–1000 °C, the TGA curves typically exhibited three major distinct weight loss regions. The first weight loss region occurred between 50 and 200 °C, which was due to the evaporation of physically adsorbed water and other volatile species from the catalyst surface [58]. This weight loss is typically small and does not significantly affect the overall performance of the catalyst. The second weight loss region occurred at higher temperatures, between 400 and 600 °C, and it was primarily due to the thermal decomposition of the catalyst components [59–61]. The catalysts exhibited another weight loss at 500–700 °C related to the decomposition of vanadium, which constitutes the active component in VWTi catalysts for SCR reactions [37]. The degree of weight loss in this region depends on the thermal stability of the catalyst and the specific reaction conditions. In the case of VWTi catalysts that have undergone thermal and hydrothermal aging, the TGA curve exhibits smaller weight loss in the second region compared to fresh catalyst. This behavior can be attributed to the aging process that has already caused some of the catalyst components, such as V_2O_5, to be lost or sintered, resulting in a lower overall weight loss during the TGA analysis. Comparing thermally aged VWTi with the same hydrothermally aged sample, the thermally aged one showed a lower weight loss. One possible reason is that thermal aging typically involves exposure to dry air, which may not result in significant water uptake by the catalyst. In contrast, hydrothermal aging involves exposure to high-temperature steam, which can lead to significant water absorption [62]. The water absorbed during hydrothermal aging can contribute to the weight loss observed in TGA, leading to a greater overall weight loss compared to thermal aging. Additionally, the structural changes that occur during thermal aging may be less harsh than those that occur during hydrothermal aging. Thermal aging typically involves exposure to high temperatures in an oxygen-containing atmosphere, which can lead to oxidation and sintering of the catalyst particles. However, the exposure to steam during hydrothermal aging can result in more severe structural changes, such as the leaching of active components, the formation of new phases, and the growth of new particles. Therefore, TGA results confirmed what was previously observed with other characterization techniques (TPR, XPS, Raman), namely that a variation in the initial composition of the VWTi catalysts occurs after thermal and hydrothermal treatments.

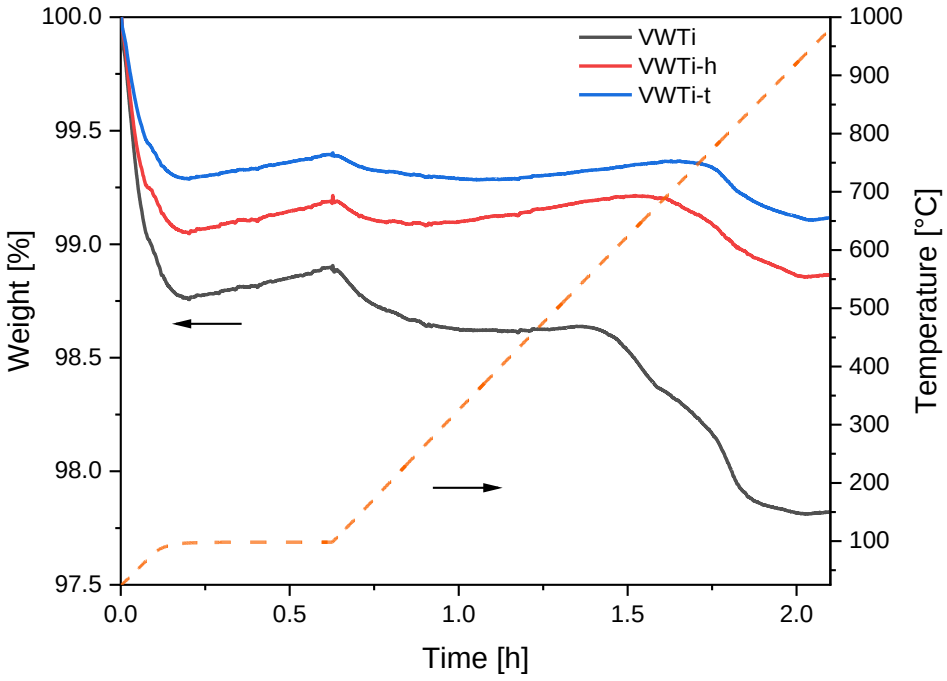

Figure 12. TGA curves of VWTi, VWTi-h and VWTi-t catalysts as function of time and temperature.

2.8. SEM/EDS

Some representative SEM images of the monolithic catalyst VWTi and its hydrothermally and thermally treated states are displayed in Figures 13 and 14, respectively.

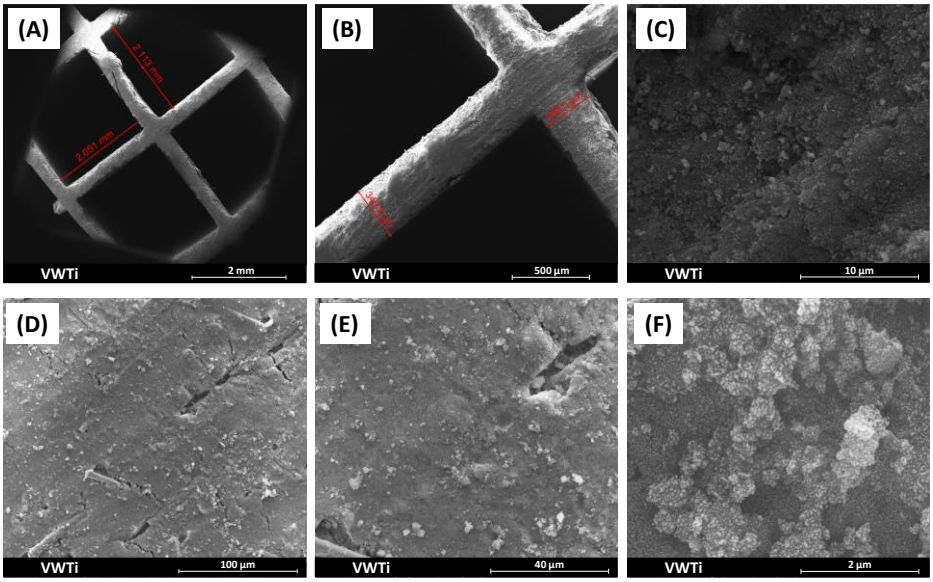

Figure 13. SEM images of fresh sample of the monolithic catalyst (VWTi) at different magnifications. (**A**–**C**) Channel section and (**D**–**F**) lateral walls of the channels.

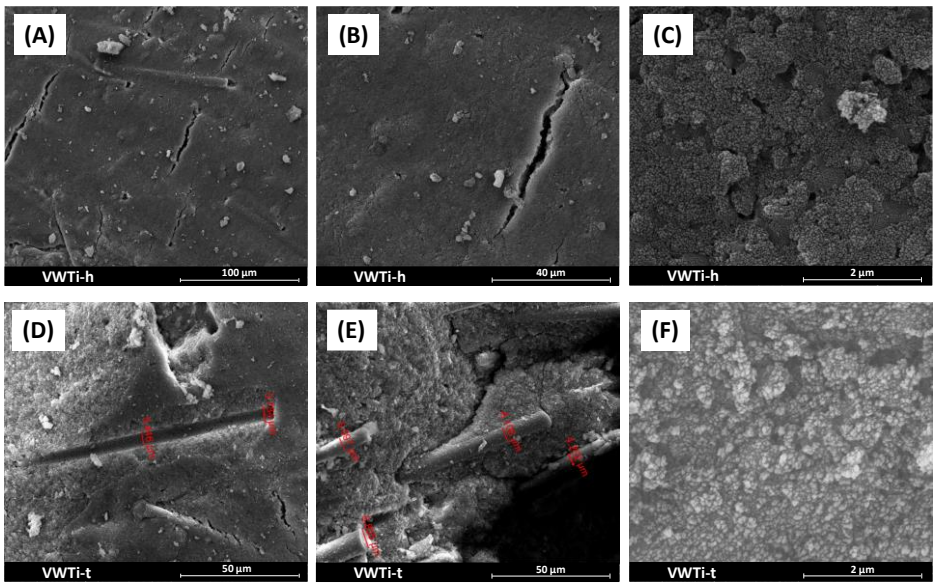

Figure 14. SEM images of lateral walls of the channels at different magnifications for monolithic catalysts. (**A**–**C**) Hydrothermally treated VWTi-h and (**D**–**F**) thermally treated VWTi-t.

SEM pictures of the channel section of the monolithic catalyst highlight that the thickness of the walls of the channels is approximately 350 microns and that the dimensions of the square channels are approximately 2 × 2 mm (Figure 13A,B). Figure 13C,F show the nanostructured nature of the monolithic catalysts, which appear to be made up of nanoparticles with size of ca. 40–45 nm. The images shown in Figure 13D,E indicate the presence of some irregularities on the lateral walls of the channels, which potentially may be due to the cutting operation required to reduce the monolithic catalyst into small pieces for SEM analysis. Notably, the glass fibers remain unseen, as they are fully covered by the catalytic material.

On the contrary, although the nanostructured nature of the monolithic catalyst was maintained (Figure 14C,F), both the hydrothermal and thermal treatments, especially the latter, resulted in the partial detachment of the catalytic material from the monolith surface. This detachment exposed certain glass fibers (see Figure 14A,E) and, in the case of thermally treated material, led to the removal of some glass fibers (see Figure 14D).

The EDX analyses revealed the presence of the three catalyst components, namely Ti, W and V, whose average percentages in the fresh sample, as well as in both the hydro- and the thermal-treated samples, were approximately 90, 8 and 2%, respectively. Consequently, the W/Ti and V/Ti ratios corresponded to 0.09 and 0.02, indicating that the amount of vanadium was almost coincident with the nominal value. In contrast, the quantity of W exceeded the nominal data. The surface segregation of tungsten, as well as vanadium, was well confirmed by XPS analysis (see Table 4). Nevertheless, the lower depth of analysis of XPS with respect to EDX was responsible for the differences found in vanadium surface concentration.

The EDX analysis carried out on the fibers left uncovered, due to the erosion in both the hydrothermally and thermally treated samples (see Figure 14A,E), highlighted their siliceous nature. Additionally, the presence of an EDX signal relating to aluminum indicated the presence of partially exposed bentonite fibers in both treated samples. Consequently, these latter two samples exhibited signs of degradation, particularly noticeable in the VWTi-t monolith.

3. Materials and Methods

3.1. Monolithic Catalyst

The catalyst (VWTi), provided by HUG Engineering AG, had a monolithic structure and a geometric parallelepiped shape (200 cpsi, with dimensions ca. 8 × 6 × 16 mm). In Table 4 the chemical composition, as certified in the data sheet, is listed.

3.2. Characterization of Monoliths

All of the characterizations were performed on small portions of the monolithic samples.

The crystalline structure of the catalyst was determined by registering powder X-ray diffraction patterns (XRD), performed on a Bruker D5000 diffractometer equipped with a Cu K anode and graphite monochromator. The data were recorded in the 20–80° 2θ range with a step size of 0.05 and time per step of 20 s. The crystalline phases were analyzed according to ICSD files (Inorganic Crystal Structure Database, FIZ Karlsruhe).

Specific surface areas and pore volumes were determined from N_2 adsorption–desorption isotherms at −196 °C using Micromeritics ASAP 2020 equipment, through the Brunauer-Emmett-Teller (BET) method in the standard pressure range 0.05–0.3 P/P^0. Before the measurements, the samples were degassed at 250 °C for 2 h. By analysis of the desorption curves, using the BJH calculation method, the pore volume and mean pore size distributions were obtained.

Hydrogen temperature programmed reduction (TPR) measurements were carried out with a Micromeritics AutoChem 2910 instrument equipped with a thermal conductivity detector (TCD). The samples (0.1 g) were pre-treated with a mixture of 5 vol% O_2 in He at 30 mL min^{-1}, heating up to 400 °C and holding at this temperature for 30 min. After cooling down to room temperature, a gas mixture of 5 vol% H_2 in Ar was introduced at 30 mL min^{-1} into the sample tube, and the temperature was increased up to 1000 °C at a rate of 10 °C min^{-1}. Hydrogen consumption values (mL g^{-1}) associated with the reduction steps were calculated by peak integration and using a calibration curve.

The X-ray photoelectron spectroscopy (XPS) analyses were performed with a VG Microtech ESCA 3000 Multilab, equipped with a dual Mg/Al anode. As excitation source, un-monochromatized Al Kα radiation (1486.6 eV) was used. The monolithic catalysts as slab were mounted on a double-sided adhesive tape. The pressure in the analysis chamber was in the range of 10^{-8} Torr during data collection. The constant charging of the samples

was removed by referencing all of the energies to the C1s binding energy set at 285.1 eV. Analyses of the peaks were performed with the CasaXPS software (Version 2.3.18PR1.0).

The Raman measurements were carried out using the second harmonic (532 nm) of an Nd:YAG laser in the backscattering mode with a Witec Alpha 300 RS instrument. For all of the analyzed samples, the power of the exciting laser was 5 mW, and the acquisition time and accumulation number were fixed, respectively, at 10 s and 10 spectra.

The thermogravimetric analyses (TGA) of the samples were registered using the TGA 1 Star System (Mettler Toledo, Scwerzenbach, Switzerland). About 10 mg of the sample was heated from room temperature to 100 C, left at this temperature for 1 h, and then heated to 1100 C at the rate of 10 C/min under flowing air at 30 mL/min.

Scanning electron microscopy (SEM) was performed using an FEI Quanta 200 ESEM microscope, operating at 20 kV. Small portions of the monolithic catalysts were glued in two different arrangements onto several stubs by using a conductive carbon cement (Agar scientific, Stansted, UK). One placement aimed to study the cross-section of the channels, while the other one was designated to investigate the morphology of the lateral walls within the channels. After this, a thin layer of gold was deposited on the samples. Moreover, an electron microprobe, used in an energy dispersive mode (EDX), was employed to obtain information on the actual Ti, W, and V composition of the monolithic catalysts.

3.3. Catalyst Activity Test

The standard NO SCR by NH_3 tests were performed in a fixed-bed continuous-flow U quartz reactor with an inner diameter of 12 mm. The feed gas, consisting of 1000 ppm NO, 1000 ppm NH_3, 10 vol% O_2 and He as balance, was led over the catalyst at a flow rate of 50 mL min^{-1} (STP), equivalent to a gas hourly space velocity (GHSV) of 5000 h^{-1}. The activities were measured as a function of temperature from 25 °C to 400 °C, with a heating rate of 5 °C min^{-1}; the data were collected after about 40 min to achieve a steady-state condition. After the VWTi monolith reached the temperature of 400 °C, the NO conversion was monitored for a total of 50 h to assess catalyst stability over an extended period (long run). In detail, the temperature was rapidly decreased from 400 °C to 350 °C, followed by steps of 25 °C down to 150 °C, maintaining each temperature for 5 h. For the more critical temperatures (350 and 200 °C), an observation period of 12 h was employed. The same monolith after the long run, labelled as VWTi-50 h, was subsequently tested again under the same conditions described at the beginning of this paragraph (standard NO SCR).

The thermal and hydrothermal aging of the monolith was carried out at 600 °C in air for 6 h with a ramp rate of 10 °C min^{-1} (thermal), and with the introduction of 30 vol% of H_2O in air (hydrothermal). The samples were identified as VWTi-t and VWTi-h, respectively. Subsequently, the aged monoliths were tested under the same conditions used for VWTi (standard NO SCR). The inlet and outlet gas compositions were analyzed by ABB detectors, infrared (Limas 11) for NO, N_2O, NO_2, and NH_3, and paramagnetic (Magnos 206) for O_2. The NO conversion and N_2 selectivity were calculated by the following equations [63]:

$$\text{NO Conversion } (\%) = \frac{[\text{NO}]_{\text{in}} - [\text{NO}]_{\text{out}}}{[\text{NO}]_{\text{in}}} \times 100 \quad (2)$$

$$\text{N}_2 \text{ Selectivity}(\%) = \left[1 - \frac{[\text{NO}_2]_{\text{out}} + 2[\text{N}_2\text{O}]_{\text{out}}}{[\text{NO}]_{\text{in}} + [\text{NH}_3]_{\text{in}} - [\text{NH}_3]_{\text{out}} - [\text{NO}]_{\text{out}}}\right] \times 100 \quad (3)$$

4. Conclusions

In the present paper, NO SCR by NH_3 was studied over a commercial monolith with composition V_2O_5-WO_3/TiO_2. The sample with typical honeycomb structure was cordierite-free, but contained glass fibers and bentonite in the structure. The catalytic tests were performed at first on the as-received catalyst (labelled as VWTi), and a long run of 50 h in the range between 150 and 350 °C was registered, showing very stable NO conversion values. Then, tests were registered after performing two aging treatments, a

thermal (sample labelled as VWTi-t) treatment at 600 °C in air for 6 h and a hydrothermal (sample labelled as VWTi-h) treatment at 600 °C for 6 h under added air flow of 30 vol% of H_2O, in order to simulate semirealistic working conditions. In the NO SCR tests, the thermally aged catalyst, VWTi-t, showed improved NO conversion at low temperature (75–200 °C) in comparison with hydrothermally aged and fresh samples, maintaining high selectivity for N_2 up to around 350 °C. Conversely, the hydrothermally treated catalyst slightly deactivated in the NO conversion at low temperature, while the selectivity for N_2 dropped above 300 °C. XPS and Raman characterizations carried out pointed to structural changes and redispersion of vanadia surface-active species that likely rearranged in a porous structure, as suggested by higher specific surface area values, with a segregation on the surface of the catalyst, thus, explaining the higher activity of this catalyst in the NO conversion, especially at low temperatures, compared to the VWT and the VWT-h samples. In the present investigation, we demonstrated that although enhanced catalytic properties were observed after thermal aging, the successful application of such a catalyst in real engine working conditions as an NO SCR device is not guaranteed. Indeed, SEM and EDX analyses evidenced that both the hydrothermal and thermal treatments, especially the latter, resulting in the partial detachment of the catalytic material from the monolith surface, led to the removal of some glass fibers and, therefore, to the degradation of the catalytic material, particularly noticeable in the VWTi-t monolith. These findings underscore the impact of the monolith matrix, glass fibers and bentonite, on the stability of the catalyst upon aging.

Author Contributions: Conceptualization, L.C., G.P. and L.F.L.; methodology, L.C., G.P., E.L.G., N.G., R.F. and S.S.; software, L.C., E.L.G. and V.L.P.; validation, L.C., G.P. and L.F.L.; formal analysis, L.C., G.P., E.L.G., V.L.P., G.M. and L.F.L.; investigation, L.C., G.P., E.L.G., V.L.P., N.G., G.M., R.F., S.S. and L.F.L.; resources, G.P. and L.F.L.; data curation, L.C., G.P., E.L.G., V.L.P., G.M., R.F., S.S. and L.F.L.; writing—original draft preparation, L.C., G.P. and L.F.L.; writing—review and editing, G.P., G.M., V.L.P., R.F., S.S. and L.F.L.; visualization, G.P. and L.F.L.; supervision, G.P. and L.F.L.; project administration, G.P. and L.F.L.; funding acquisition, G.P. and L.F.L. All authors have read and agreed to the published version of the manuscript.

Funding: This work was funded by the project TECBIA "Tecnologie a Basso Impatto Ambientale per la produzione di energia sui mezzi navali" (Project n. F.090041/01/X36) and by the Project ARS01_00334 NAUSICA "NAvi efficienti tramite l'Utilizzo di Soluzioni tecnologiche Innovative e low CArbon" – CUP B45F21000680005.

Data Availability Statement: The data presented in this study are available on request from the corresponding authors.

Acknowledgments: The authors are grateful to Luca Pinauda (Hug Engineering AG) for providing the commercial monolithic catalyst. G. Napoli (ISMN-CNR) is acknowledged for support in the financial management of the TECBIA and NAUSICA projects, F. Giordano (ISMN-CNR, Italy) is acknowledged for carrying out XRD measurements, and M. Condorelli (University of Catania) is acknowledged for Raman analyses.

Conflicts of Interest: The authors declare no conflicts of interest.

References

1. Chu, B.; Ma, Q.; Liu, J.; Ma, J.; Zhang, P.; Chen, T.; Feng, Q.; Wang, C.; Yang, N.; Ma, H.; et al. Air Pollutant Correlations in China: Secondary Air Pollutant Responses to NO_x and SO_2 Control. *Environ. Sci. Technol. Lett.* **2020**, *7*, 695–700. [CrossRef]
2. Napolitano, P.; Liotta, L.F.; Guido, C.; Tornatore, C.; Pantaleo, G.; La Parola, V.; Beatrice, C. Insights of Selective Catalytic Reduction Technology for Nitrogen Oxides Control in Marine Engine Applications. *Catalysts* **2022**, *12*, 1191. [CrossRef]
3. Koebel, M.; Elsener, M.; Kleemann, M. Urea-SCR: A Promising Technique to Reduce NO_x Emissions from Automotive Diesel Engines. *Catal. Today* **2000**, *59*, 335–345. [CrossRef]
4. Selleri, T.; Gramigni, F.; Nova, I.; Tronconi, E. NO Oxidation on Fe- and Cu-Zeolites Mixed with BaO/Al_2O_3: Free Oxidation Regime and Relevance for the NH_3-SCR Chemistry at Low Temperature. *Appl. Catal. B Environ.* **2018**, *225*, 324–331. [CrossRef]

5. Colombo, M.; Nova, I.; Tronconi, E. A Comparative Study of the NH_3-SCR Reactions over a Cu-Zeolite and a Fe-Zeolite Catalyst. *Catal. Today* **2010**, *151*, 223–230. [CrossRef]
6. Sitshebo, S.; Tsolakis, A.; Theinnoi, K.; Rodríguez-Fernández, J.; Leung, P. Improving the Low Temperature NO_x Reduction Activity over a Ag-Al_2O_3 Catalyst. *Chem. Eng. J.* **2010**, *158*, 402–410. [CrossRef]
7. Liu, W.; Long, Y.; Liu, S.; Zhou, Y.; Tong, X.; Yin, Y.; Li, X.; Hu, K.; Hu, J. Commercial SCR Catalyst Modified with Different Noble Metals (Ag, Pt, Pd) to Efficiently Remove Slip Ammonia and NO_x in the Flue Gas. *J. Taiwan Inst. Chem. Eng.* **2022**, *138*, 104472. [CrossRef]
8. Lietti, L.; Nova, I.; Ramis, G.; Dall'Acqua, L.; Busca, G.; Giamello, E.; Forzatti, P.; Bregani, F. Characterization and Reactivity of V_2O_5-MoO_3/TiO_2 De-NOx SCR Catalysts. *J. Catal.* **1999**, *187*, 419–435. [CrossRef]
9. Liu, S.; Wang, H.; Zhang, R.; Wei, Y. Synergistic Effect of Niobium and Ceria on Anatase for Low-Temperature NH_3-SCR of NO Process. *Mol. Catal.* **2019**, *478*, 110563. [CrossRef]
10. Zhu, L.; Zhong, Z.; Xue, J.; Xu, Y.; Wang, C.; Wang, L. NH_3-SCR Performance and the Resistance to SO_2 for Nb Doped Vanadium Based Catalyst at Low Temperatures. *J. Environ. Sci.* **2018**, *65*, 306–316. [CrossRef] [PubMed]
11. Zhang, J.; Bi, Z.; Liang, Y. Development of a Nutrient Recipe for Enhancing Methane Release from Coal in the Illinois Basin. *Int. J. Coal Geol.* **2018**, *187*, 11–19. [CrossRef]
12. Forzatti, P. Present Status and Perspectives in De-NO_x SCR Catalysis. *Appl. Catal. A Gen.* **2001**, *222*, 221–236. [CrossRef]
13. Kompio, P.G.W.A.; Brückner, A.; Hipler, F.; Auer, G.; Löffler, E.; Grünert, W. A New View on the Relations between Tungsten and Vanadium in $V_2O_5WO_3$/TiO_2 Catalysts for the Selective Reduction of NO with NH_3. *J. Catal.* **2012**, *286*, 237–247. [CrossRef]
14. Kompio, P.G.W.A.; Brückner, A.; Hipler, F.; Manoylova, O.; Auer, G.; Mestl, G.; Grünert, W. V_2O_5-WO_3/TiO_2 Catalysts under Thermal Stress: Responses of Structure and Catalytic Behavior in the Selective Catalytic Reduction of NO by NH_3. *Appl. Catal. B Environ.* **2017**, *217*, 365–377. [CrossRef]
15. Amiridis, M.D.; Duevel, R.V.; Wachs, I.E. The Effect of Metal Oxide Additives on the Activity of V_2O_5/TiO_2 Catalysts for the Selective Catalytic Reduction of Nitric Oxide by Ammonia. *Appl. Catal. B Environ.* **1999**, *20*, 111–122. [CrossRef]
16. Fierro, J.L.G. *Metal Oxides: Chemistry and Applications*; CRC Press: Boca Raton, FL, USA, 2005; ISBN 978-1-4200-2812-6.
17. Wachs, I.E. Recent Conceptual Advances in the Catalysis Science of Mixed Metal Oxide Catalytic Materials. *Catal. Today* **2005**, *100*, 79–94. [CrossRef]
18. Forzatti, P.; Lietti, L. Recent advances in de-NOxing catalysis for stationary applications. *Heterog. Chem. Rev.* **1996**, *3*, 33–51. [CrossRef]
19. Li, J.; Fu, H.; Fu, L.; Hao, J. Preparation of Metallic Ion-Doped TiO_2 Thin Films and Their Photocatalytic Performance for Toluene Degradation. *Chin. J. Catal.* **2005**, *26*, 503–507.
20. Chapman, D.M. Behavior of Titania-Supported Vanadia and Tungsta SCR Catalysts at High Temperatures in Reactant Streams: Tungsten and Vanadium Oxide and Hydroxide Vapor Pressure Reduction by Surficial Stabilization. *Appl. Catal. A Gen.* **2011**, *392*, 143–150. [CrossRef]
21. Nunney, M.J. *Light and Heavy Vehicle Technology*, 4th ed.; Routledge: London, UK, 2008; ISBN 9780080465753.
22. Liu, X.; Chen, H.; Wu, X.; Cao, L.; Jiang, P.; Yu, Q.; Ma, Y. Effects of SiO_2 Modification on the Hydrothermal Stability of the V_2O_5/WO_3-TiO_2 NH_3-SCR Catalyst: TiO_2 Structure and Vanadia Species. *Catal. Sci. Technol.* **2019**, *9*, 3711–3720. [CrossRef]
23. Liu, J.; He, G.; Shan, W.; Yu, Y.; Huo, Y.; Zhang, Y.; Wang, M.; Yu, R.; Liu, S.; He, H. Introducing Tin to Develop Ternary Metal Oxides with Excellent Hydrothermal Stability for NH_3 Selective Catalytic Reduction of NOx. *Appl. Catal. B Environ.* **2021**, *291*, 120125. [CrossRef]
24. Species, S.; Joint, S.K.; Control, P. DRIFT Study on Cerium—Tungsten/Titiania Catalyst for Selective Catalytic Reduction of NO_x with NH_3. *Environ. Sci. Technol.* **2010**, *44*, 9590–9596.
25. Bartholomew, C.H. Mechanisms of Catalyst Deactivation. *Appl. Catal. A Gen.* **2001**, *212*, 17–60. [CrossRef]
26. Djerad, S.; Tifouti, L.; Crocoll, M.; Weisweiler, W. Effect of vanadia and tungsten loadings on the physical and chemical characteristics of V_2O_5-WO_3/TiO_2 catalysts. *J. Mol. Catal. A Chem.* **2004**, *208*, 257–265. [CrossRef]
27. Lough, G.C.; Schauer, J.J.; Park, J.S.; Shafer, M.M.; Deminter, J.T.; Weinstein, J.P. Emissions of Metals Associated with Motor Vehicle Roadways. *Environ. Sci. Technol.* **2005**, *39*, 826–836. [CrossRef]
28. Barceloux, D.G. Vanadium. *J. Toxicol. Clin. Toxicol.* **1999**, *37*, 265–278. [CrossRef]
29. Costigan, M.; Cary, R.; Dobson, S. Concise International Chemical Assessment Document 29: Vanadium Pentoxide and Other Inorganic Vanadium Compounds; Geneva, 2001; ISBN 92 4 153029 4.
30. Madia, G.; Elsener, M.; Koebel, M.; Raimondi, F.; Wokaun, A. Thermal Stability of Vanadia-Tungsta-Titania Catalysts in the SCR Process. *Appl. Catal. B Environ.* **2002**, *39*, 181–190. [CrossRef]
31. Nova, I.; Dall'Acqua, L.; Lietti, L.; Giamello, E.; Forzatti, P. Study of Thermal Deactivation of a De-NO_x Commercial Catalyst. *Appl. Catal. B Environ.* **2001**, *35*, 31–42. [CrossRef]
32. Marberger, A.; Elsener, M.; Ferri, D.; Kröcher, O. VOx Surface Coverage Optimization of V_2O_5/WO_3-TiO_2 SCR Catalysts by Variation of the V Loading and by Aging. *Catalysts* **2015**, *5*, 1704–1720. [CrossRef]
33. Amiridis, M.D.; Solar, J.P. Selective Catalytic Reduction of Nitric Oxide by Ammonia over V_2O_5/TiO_2, V_2O_5/TiO_2/SiO_2, and V_2O_5-WO_3/TiO_2 Catalysts: Effect of Vanadia Content on the Activation Energy. *Ind. Eng. Chem. Res.* **1996**, *35*, 978–981. [CrossRef]

34. Wachs, I.E.; Deo, G.; Weckhuysen, B.M.; Andreini, A.; Vuurman, M.A.; De Boer, M.; Amiridis, M.D. Selective Catalytic Reduction of NO with NH_3 over Supported Vanadia Catalysts. *J. Catal.* **1996**, *161*, 211–221. [CrossRef]
35. Girard, J.W.; Montreuil, C.; Kim, J.; Cavataio, G.; Lambert, C. Technical Advantages of Vanadium SCR Systems for Diesel NO_x Control in Emerging Markets. *SAE Int. J. Fuels Lubr.* **2008**, *1*, 488–494. [CrossRef]
36. Asako, T.; Kai, R.; Toyoshima, T.; Vogt, C.; Hirose, S.; Nakao, S. *Evaluation of Hydrothermally Aged Vanadia SCR on High-Porosity Substrate*; SAE Technical Paper; SAE International: Warrendale, PA, USA, 2016. [CrossRef]
37. Rasmussen, S.B.; Abrams, B.L. Fundamental Chemistry of V-SCR Catalysts at Elevated Temperatures. *Catal. Today* **2017**, *297*, 60–63. [CrossRef]
38. Maunula, T.; Kinnunen, T.; Kanniainen, K.; Viitanen, A.; Savimaki, A. *Thermally Durable Vanadium-SCR Catalysts for Diesel Applications*; SAE Technical Paper; SAE International: Warrendale, PA, USA, 2013; Volume 2. [CrossRef]
39. Lin, C.H.; Bai, H. Adsorption Behavior of Moisture over a Vanadia/Titania Catalyst: A Study for the Selective Catalytic Reduction Process. *Ind. Eng. Chem. Res.* **2004**, *43*, 5983–5988. [CrossRef]
40. Wang, C.; Yang, S.; Chang, H.; Peng, Y.; Li, J. Dispersion of Tungsten Oxide on SCR Performance of $V_2O_5WO_3/TiO_2$: Acidity, Surface Species and Catalytic Activity. *Chem. Eng. J.* **2013**, *225*, 520–527. [CrossRef]
41. Li, J.; Chang, H.; Ma, L.; Hao, J.; Yang, R.T. Low-Temperature Selective Catalytic Reduction of NO_x with NH_3 over Metal Oxide and Zeolite Catalysts—A Review. *Catal. Today* **2011**, *175*, 147–156. [CrossRef]
42. Beale, A.M.; Lezcano-Gonzalez, I.; Maunula, T.; Palgrave, R.G. Development and Characterization of Thermally Stable Supported V–W–TiO_2 Catalysts for Mobile NH_3–SCR Applications. *Catal. Struct. React.* **2015**, *1*, 25–34. [CrossRef]
43. Besselmann, S.; Freitag, C.; Hinrichsen, O.; Muhler, M. Temperature-Programmed Reduction and Oxidation Experiments with V_2O_5/TiO_2 Catalysts. *Phys. Chem. Chem. Phys.* **2001**, *3*, 4633–4638. [CrossRef]
44. Ousmane, M.; Liotta, L.F.; Di Carlo, G.; Pantaleo, G.; Venezia, A.M.; Deganello, G.; Retailleau, L.; Boreave, A.; Giroir-Fendler, A. Supported Au Catalysts for Low-Temperature Abatement of Propene and Toluene, as Model VOCs: Support Effect. *Appl. Catal. B Environ.* **2011**, *101*, 629–637. [CrossRef]
45. Mdlovu, N.V.; Yang, N.C.; Lin, K.S.; Chang, C.J.; Dinh, K.T.; Lin, Y.G. Formulation and Characterization of W-Doped Titania Nanotubes for Adsorption/Photodegradation of Methylene Blue and Basic Violet 3 Dyes. *Catal. Today* **2022**, *388–389*, 36–46. [CrossRef]
46. Komornicki, S.; Radecka, M.; Sobaś, P. Structural Properties of TiO_2-WO_3 Thin Films Prepared by r.f. Sputtering. *J. Mater. Sci. Mater. Electron.* **2004**, *15*, 527–531. [CrossRef]
47. Hu, J.; Lei, Y.; Yuan, M.; Lin, Y.; Jiang, Z.; Ouyang, Z.; Du, P.; Wu, Y. Enhanced Photoelectric Performance of GQDs Anchored WO_3 with a "dot-on-Nanoparticle" Structure. *Mater. Res. Express* **2020**, *7*, 75602. [CrossRef]
48. Zakharova, G.S.; Podval'Naya, N.V.; Kuznetsov, M.V. XPS Study of Nanorods of Doped Vanadium Oxide $M_xV_2O_5{\cdot}nH_2O$ (M = Na, K, Rb, Cs). *Russ. J. Inorg. Chem.* **2011**, *56*, 267–272. [CrossRef]
49. Chenakin, S.P.; Silvy, R.P.; Kruse, N. X-ray Induced Surface Modification of Aluminovanadate Oxide. *Catal. Lett.* **2005**, *102*, 39–43. [CrossRef]
50. Schuhl, Y.; Baussart, H.; Delobel, R.; Le Bras, M.; Leroy, J.M.; Gengembre, L.; Grimblot, J. Study of Mixed-Oxide Catalysts Containing Bismuth, Vanadium and Antimony. Preparation, Phase Composition, Spectroscopic Characterization and Catalytic Oxidation of Propene. *J. Chem. Soc. Faraday Trans. 1 Phys. Chem. Condens. Phases* **1983**, *79*, 2055–2069. [CrossRef]
51. Palcheva, R.; Dimitrov, L.; Tyuliev, G.; Spojakina, A.; Jiratova, K. TiO_2 Nanotubes Supported NiW Hydrodesulphurization Catalysts: Characterization and Activity. *Appl. Surf. Sci.* **2013**, *265*, 309–316. [CrossRef]
52. Cheng, P.; Deng, C.S.; Liu, D.N.; Dai, X.M. Titania Surface Modification and Photovoltaic Characteristics with Tungsten Oxide. *Appl. Surf. Sci.* **2008**, *254*, 3391–3396. [CrossRef]
53. Caravaca, M.; Morales, J.J.; Abad, J. Interaction of NO with SiO_x/TiO_2 (1 1 0)-(1 × 2). *Appl. Surf. Sci.* **2021**, *551*, 2–6. [CrossRef]
54. Liu, B.; Du, J.; Lv, X.; Qiu, Y.; Tao, C. Washcoating of Cordierite Honeycomb with Vanadia-Tungsta-Titania Mixed Oxides for Selective Catalytic Reduction of NO with NH_3. *Catal. Sci. Technol.* **2015**, *5*, 1241–1250. [CrossRef]
55. Wachs, I.E. Raman and IR Studies of Surface Metal Oxide Species on Oxide Supports: Supported Metal Oxide Catalysts. *Catal. Today* **1996**, *27*, 437–455. [CrossRef]
56. Li, G.; Li, L.; Boerio-Goates, J.; Woodfield, B.F. High Purity Anatase TiO_2 Nanocrystals: Near Room-Temperature Synthesis, Grain Growth Kinetics, and Surface Hydration Chemistry. *J. Am. Chem. Soc.* **2005**, *127*, 8659–8666. [CrossRef]
57. Fiorenza, R.; Bellardita, M.; D'Urso, L.; Compagnini, G.; Palmisano, L.; Scirè, S. Au/TiO_2-CeO_2 Catalysts for Photocatalytic Water Splitting and VOCs Oxidation Reactions. *Catalysts* **2016**, *6*, 121. [CrossRef]
58. Xu, T.; Wu, X.; Gao, Y.; Lin, Q.; Hu, J.; Weng, D. Comparative Study on Sulfur Poisoning of V_2O_5-Sb_2O_3/TiO_2 and V_2O_5-WO_3/TiO_2 Monolithic Catalysts for Low-Temperature NH_3-SCR. *Catal. Commun.* **2017**, *93*, 33–36. [CrossRef]
59. Cimino, S.; Ferone, C.; Cioffi, R.; Perillo, G.; Lisi, L. A Case Study for the Deactivation and Regeneration of a V_2O_5-WO_3/TiO_2 Catalyst in a Tail-End SCR Unit of a Municipal Waste Incineration Plant. *Catalysts* **2019**, *9*, 464. [CrossRef]
60. Liu, H.; Fan, Z.; Sun, C.; Yu, S.; Feng, S.; Chen, W.; Chen, D.; Tang, C.; Gao, F.; Dong, L. Improved Activity and Significant SO_2 Tolerance of Samarium Modified CeO_2-TiO_2 Catalyst for NO Selective Catalytic Reduction with NH_3. *Appl. Catal. B Environ.* **2019**, *244*, 671–683. [CrossRef]
61. Xu, T.; Wu, X.; Liu, X.; Cao, L.; Lin, Q.; Weng, D. Effect of Barium Sulfate Modification on the SO_2 Tolerance of V_2O_5/TiO_2 Catalyst for NH_3-SCR Reaction. *J. Environ. Sci.* **2017**, *57*, 110–117. [CrossRef]

62. Lisi, L.; Cimino, S. *Catalysts Deactivation, Poisoning and Regeneration*; MDPI: Basel, Switzerland, 2019; ISBN 9783039215461.
63. Liu, W.; Long, Y.; Zhou, Y.; Liu, S.; Tong, X.; Yin, Y.; Li, X.; Hu, K.; Hu, J. Excellent Low Temperature NH_3-SCR and NH_3-SCO Performance over Ag-Mn/Ce-Ti Catalyst: Evaluation and Characterization. *Mol. Catal.* **2022**, *528*, 112510. [CrossRef]